Turkish Journal of Chemistry
http://journals.tubitak.gov.tr/chem/
Research Article

Turk J Chem
(2015) 39: 683 – 696

doi:10.3906/kim-1411-17

Sustainable activity of hydrothermally synthesized mesoporous silicates in acetic acid esterification

Veli ŞİMŞEK[1], Levent DEĞİRMENCİ[1,*], Kırali MÜRTEZAOĞLU[2]
[1]Chemical and Process Engineering Department, Bilecik Seyh Edebali University, Gulumbe Campus, Bilecik, Turkey
[2]Chemical Engineering Department, Gazi University, Maltepe, Ankara, Turkey

Received: 07.11.2014 • **Accepted/Published Online:** 06.03.2015 • **Printed:** 30.06.2015

Abstract: A hydrothermal method was applied in the synthesis of mesoporous silicates containing silicotungstic acid (STA). The synthesis procedures were developed by modification of procedures previously applied in the synthesis of MCM-41 and SBA-15. The synthesized catalysts were named MCM-41-S and SBA-15-S based on MCM-41 and SBA-15. Their activities were investigated in ethyl acetate production, which was selected as the model reaction. The results indicated that the activity of SBA-15-S catalysts increased with increasing STA in the catalyst. Reaction experiments were also conducted in identical conditions in the presence of catalysts recovered after the reaction. The results indicated that sustainable activity could be achieved in the presence of these spent catalysts with activity losses around 10%. Evaluation of characterization analyses conducted with fresh and spent catalysts showed that the activity loss of SBA-15-S catalysts had merely been due to STA leaching, whereas deformation of pore structure had occurred in MCM-41-S catalysts.

Key words: Mesoporous silicate, silicotungstic acid, hydrothermal method, sustainable activity, ethyl acetate

1. Introduction

The synthesis of catalysts loaded on various supports has attracted increased attention in recent years. These catalysts exhibit high activities in various reactions due to the high area of interaction provided by the support material. A literature survey revealed the use of various templates as support materials. Zeolites, SiO_2, alumina, and activated carbon are among the templates used in catalyst syntheses.[1–5] The surface area of these templates can be as high as 700 m^2/g, which provides a suitable medium for homogeneous dispersion of active material throughout the template.[6] However, the pore size of the catalysts synthesized with these templates have a maximum value of 1 nm and this prevents incorporation of bigger active materials inside the channels of the template.[4]

Silicate structured mesoporous materials with larger surface areas and narrow pore size distributions are fine candidates for application as support materials in catalytic synthesis. Use of these materials as catalyst supports dates back to the discovery of the mesoporous M41S family with ordered pore size of 8 nm.[4] SBA-15, the latest mesoporus material discovered, has hexagonal pores between 5 and 15 nm.[7]

Application of MCM-41 and SBA-15 solely as catalyst is unlikely due to their weak Lewis acidity and the absence of Brønsted acid sites. Therefore, Brønsted acidity should be enhanced by either impregnation or framework modification with strong acid species.[8,9]

*Correspondence: levent.degirmenci@bilecik.edu.tr

Heteropoly acids (HPAs) constitute an important catalyst alternative for reactions that require strong Brønsted acidity.[10] Their acidity is comparable to that of mineral acids such as H_2SO_4 and HCl.[10,11] Investigations on these compounds have increased following their successful application in alcohol dehydration, ethyl tertiary butyl ether (ETBE) synthesis, and esterification reactions.[10–14] However, the surface area of these catalysts is very low (>1 m^2/g), which results in low activity in reactions.[13] These compounds are highly soluble in liquid phase, especially in the presence of polar compounds, which limits their use in vapor phase applications due to their loss in reaction media.[11–13,15] Moreover, regeneration of HPAs is difficult to achieve as a result of their relatively low thermal stability. Hence, improvement in the activity of HPAs could be achieved by impregnating them into certain support materials such as MCM-41 and SBA-15.[12,15,16]

Impregnation is a popular method utilized in incorporation of HPAs onto MCM-41 and SBA-15.[15,17–20] The synthesized catalysts were tested in a variety of reactions including isopropylation of naphthalene with isopropanol, benzylation and alkylation of phenol, and esterification of acetic acid with ethanol and n-butanol.[15,17–20] It was reported by Liu et al. that the catalytic performance of catalysts prepared by impregnation onto SBA-15 was higher than those prepared by impregnation onto MCM-41 and amorphous silica.[17] A similar conclusion was reached by Sawant et al.[18,19] They stated that SBA-15 retained its mesostructure despite the high HPA loading and calcination temperature applied in the study.[18,19] Loading amount of HPA during catalyst synthesis is an important parameter in maintaining high activity in reactions. The results obtained by Kumar et al.[20] clearly indicated that the highest activity and selectivity might be reached in lower HPA loadings, which also indicated that dispersion of the active material throughout the support was equally important.[20]

Alternative methods such as sol-gel and the hydrothermal method have also been used in catalyst syntheses. These methods have been compared with the impregnation method by Li et al.[15] and Yang et al.[21] It was stated that sol-gel derived SBA-15/HPA composite was more stable in terms of acidity and structural regularity and catalytic tests to determine reusability revealed better performance of these catalysts.[21] Similar results were obtained by Li et al.[15] with better dispersion of polyoxometalates on MCM-41 compared to impregnated catalysts. Results also indicated that the mesoporous structure remained intact after synthesis. These catalysts also showed better catalytic performance and reusability than those synthesized by impregnation.[21]

Ethyl esters have long been considered alternatives to biodiesel additives. Certain properties of these compounds such as net standard enthalpy of combustion and freezing point are comparable to those of vegetable oil fatty ester biodiesels. These properties enable ethyl esters to be utilized as biodiesel additives.[22] Ethyl acetate production is conducted in the presence of a variety of catalysts including silica gel supported phosphomolybdic acid and alkali promoted HPA impregnated on montmorillonite K10.[23,24] Activities of HPA impregnated catalysts varied according to loading amounts of active material. In the work by El-Wahab and Said, a loading amount varying between 1% and 30% was applied for catalyst syntheses.[23] Among these catalysts the highest activity was obtained as 65% with a catalyst loading of 10%. In the work by Gurav and Bokade, yield and selectivity of ethyl acetate were determined as 90% and 100%, respectively.[24] These values were obtained with a loading of 20% dodecotungstophosphoric acid catalysts on K10 montmorillonite.[24]

In the present study STA was incorporated into MCM-41 and SBA-15 based mesoporous materials by hydrothermal method. The synthesized catalysts were tested in ethyl acetate production selected as the model reaction. Physical properties of the catalysts were determined by XRD, N_2 adsorption–desorption, BET, SEM, and EDX analyses. Reusability of the catalysts was determined by reaction experiments conducted in the presence of the catalysts recovered from the reaction media. The changes in their physical properties were

determined by evaluation of reaction experiments and characterization studies of reused catalysts in accordance.

Ethyl acetate reaction in liquid phase was especially selected as the model reaction to imitate harsh conditions that catalysts would face during a reaction. Catalysts synthesized with incorporation of active material into a support structure generally face one of two problems. When used in reactions, the active material of the catalyst may dissolve and migrate to the reaction media, resulting in loss of activity in repeated use or the reactants diffusing into the porous network may cause deformation or even destruction of the pore structure, preventing long-term application of the catalyst. Ethanol used as reactant in reaction experiments is a polar solvent that dissolves HPA in the liquid phase. The hydrothermal method requires simultaneous addition of active material during the synthesis of support. Silicotungstic acid, used as the active material, is expected to behave as a secondary silica source that, in our opinion, will facilitate incorporation of the active material inside the channels of the catalyst. One of the advantages of the method is the amount of active material used in the synthesis. In general, the highest amount of loading in synthesis was 10% and considerable activities in the presence of these catalysts were reported. As a result of the entrapment of active material inside the mesoporous channels of the catalyst, it is expected to prevent or decrease leaching of HPA to a certain extent, which is the most important highlight of the study. It is also expected that the catalysts would preserve their molecular configuration after repeated use. The loading contents of STA were varied between 1.25% and 5% based on weight ratio of tungsten (W) of STA and silica of sodium silicate for MCM-41 based materials and tetra ethyl ortho silicate (TEOS) for SBA-15 based materials. Parent MCM-41 and SBA-15 were also synthesized and analyzed to obtain a comparison of catalysts' physical properties along with the changes in molecular structure due to STA incorporation. MCM-41-S and SBA-15-S were selected as abbreviations for MCM-41 and SBA-15 based catalysts to enable easy follow-up of the results.

2. Results and discussion

2.1. Reaction experiments

Ethyl acetate production was conducted at 343 K and in the presence of 0.4 g catalyst loading. Catalysts were recovered from the reaction medium and reused under identical conditions after being washed with deionized water and dried at 90 °C for 3 h. Blank experiments without catalyst were also conducted to investigate the possibility of autocatalysis with acetic acid. The highest acetic acid conversion obtained was 0.05 at the end of 270 min, indicating a negligible effect of acetic acid on catalyst activity. Acetic acid conversions obtained in the presence of MCM-41-S and SBA-15-S catalysts between 15 and 270 min are given in Figures 1a and 1b, respectively. A nonmonotonic dependence of %W/Si loading on acetic acid conversion was observed in the presence of MCM-41-S catalysts (Figure 1a), whereas acetic acid conversion increased with increasing W/Si % ratios in the presence of SBA-15-S catalysts (Figure 1b). Evaluation of conversion values obtained in the presence of MCM-41-S catalysts revealed a negligible change in conversion with increasing STA loading, implying dependence of catalyst activity on the amount of diffusing STA inside the pores. The increase in acetic acid conversion values after 150 min was thought to be due to migration of STA, agglomerated on the mesoporous structure, to the reaction solution and acted as a homogeneous catalyst (Figure 1a). On the other hand, a steady increase in acetic acid conversion was observed with increasing STA amount in the presence of SBA-15-S catalysts (Figure 1b). There are many reports in the literature stating thicker pore walls, wider pore sizes, and higher hydrothermal stability of SBA-15 compared to MCM-41.[17,20,21,25] Hence the increase in acetic acid conversion in the presence of SBA-15-S catalysts implied homogeneous dispersion of greater STA amounts inside the pores of the catalyst.

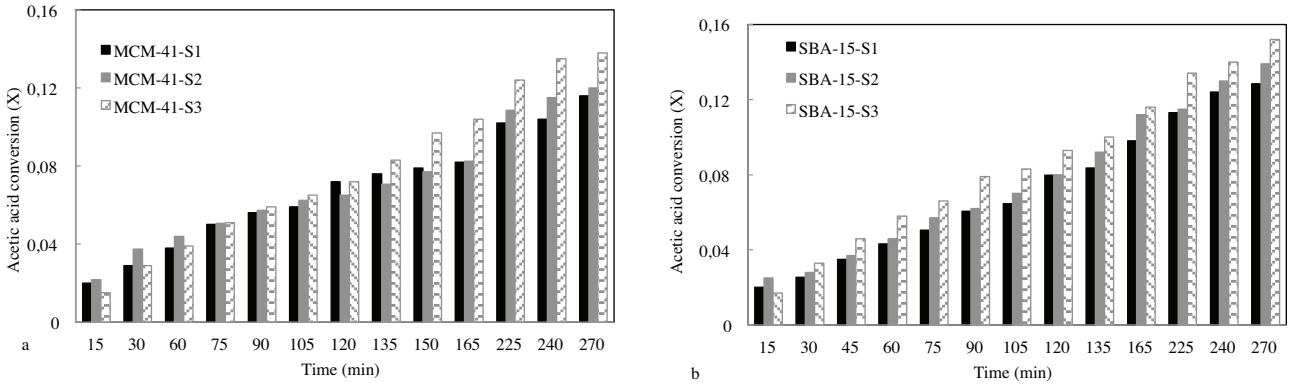

Figure 1. Effect of W/Si % ratios on acetic acid conversions obtained in the presence of a) MCM-41-S and b) SBA-15-S catalysts.

The reusability of catalysts was determined by evaluation of reaction experiments conducted under identical conditions and in the presence of recovered catalysts. Both MCM-41-S (Figures 2a–2c) and SBA-15-S (Figures 3a–3c) catalysts exhibited the highest activity losses with 5% W/Si loading. This result implied agglomeration of STA on the surface of catalyst. In order to determine the extent of activity loss, acetic acid conversion obtained at the end of 270 min was taken into account and reusability of the catalysts was compared accordingly. Activity losses of MCM-41-S catalysts at the end of the second run were 1.72%, 8.3%, and 13% for MCM-41-S1, MCM-41-S2, and MCM-41-S3 catalysts, respectively (Figures 2a–2c). Activity losses of SBA-15-S catalysts at the end of the second run were 9.7%, 10.8%, and 14.5% in the presence of SBA-15-S1, SBA-15-S2, and SBA-15-S3 catalysts, respectively (Figure 3a–3c). The results indicated the reusability of both catalysts in liquid phase reactions.

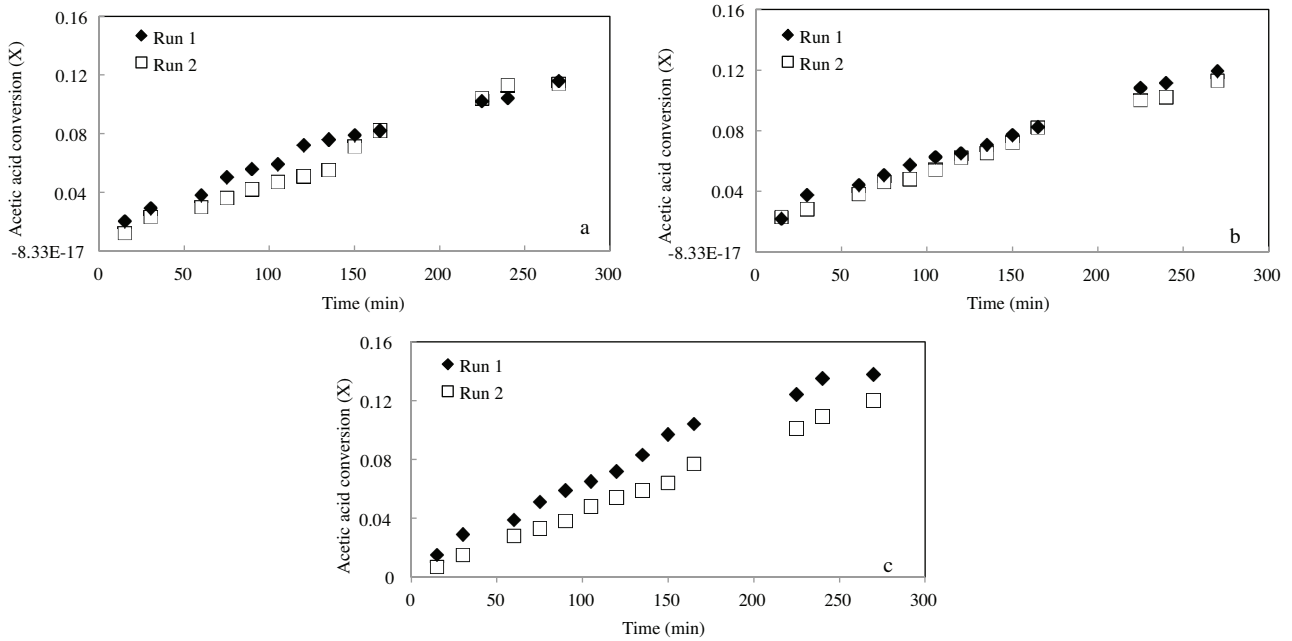

Figure 2. Acetic acid conversions obtained in the presence of fresh (Run 1) and spent (Run 2) a) MCM-41-S1 b) MCM-41-S2 and c) MCM-41-S3 catalysts (reaction temperature: 343 K; catalyst loading: 0.4 g).

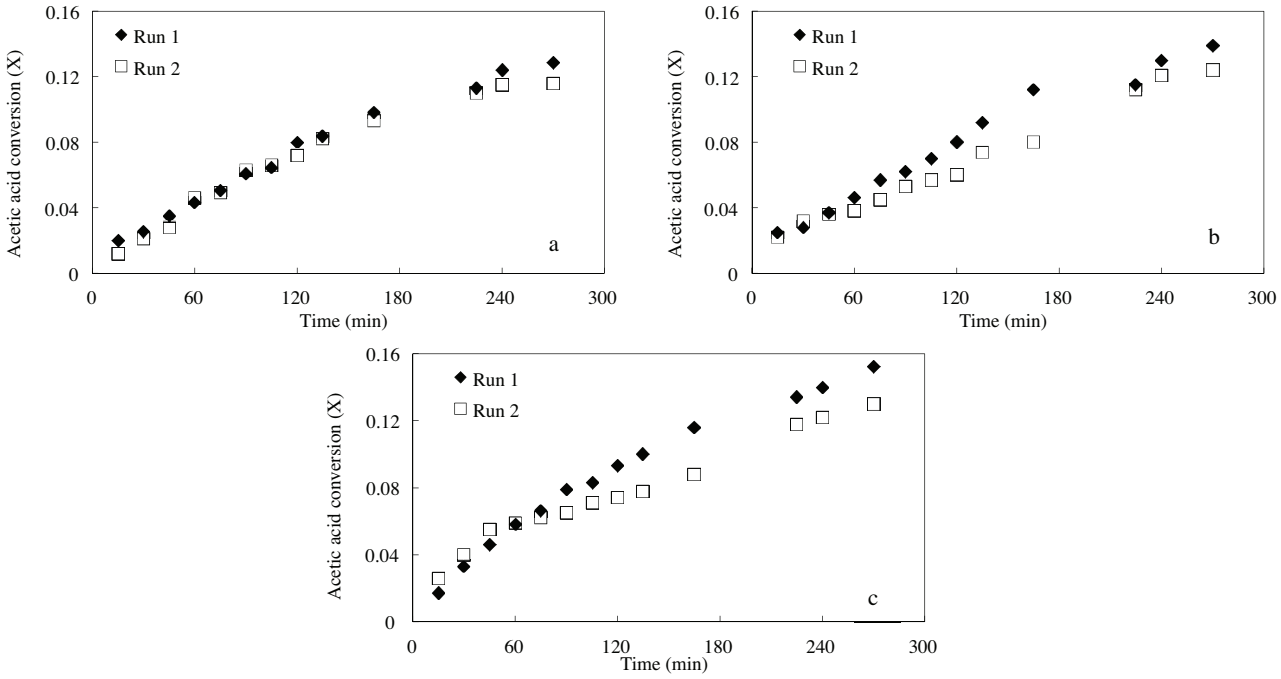

Figure 3. Acetic acid conversions obtained in the presence of fresh (Run 1) and spent (Run 2) a) SBA-15-S1 b) SBA-15-S2 and c) SBA-15-S3 catalysts (reaction temperature: 343 K; catalyst loading: 0.4 g).

Reaction experiments conducted in the presence of recovered catalysts indicated sustainable activity of both catalysts. In the case of SBA-15-S catalysts, the loss of activity was mainly due to leaching of STA, on the external surface of the catalyst, to the reaction mixture. It was concluded for SBA-15-S catalysts that the amount of STA lost during the reaction was negligible provided that the active material remained inside the pores of the catalyst (Figures 3a–3c). The hydrothermal method was concluded to be an effective method for placing the active material inside the pores of the structure and preventing activity loss of the catalyst due to leaching of active material.

2.2. Characterization studies

DRIFT spectra of pyridine adsorbed MCM-41-S and SBS-15-S catalysts are illustrated in Figures 4a and 4b, respectively. The presence of Lewis and Brønsted acid sites indicating the acidic characteristics of catalysts was determined by identification of peaks at 1441 and 1591 cm^{-1} for both catalysts. The peaks observed at 1485 cm^{-1} were attributed to physically adsorbed pyridine (Figures 4a and 4b).[8,13,26,27] The locations of Lewis and Brønsted acid sites are identical as both catalysts exhibited identical hexagonal structures. The ratios of peak areas determining Lewis and Brønsted acid sites were calculated in terms of B/L ratio, which were 0.97, 0.99, and 1.16 for MCM-41-S catalysts (Figure 4a). These ratios were determined as 0.95, 0.62, and 1.13 for SBA-15-S catalysts (Figure 4b). The results indicated an increase in the acidity with increasing amount of STA in the catalyst structure (Figures 4a and 4b).

The low angle XRD patterns of MCM-41 and MCM-41-S catalysts and high angle XRD patterns of STA and MCM-41-S catalysts are illustrated in Figures 5a and 5b, respectively. The peak values of MCM-41 obtained at 2.34, 4.03, 4.64, and 6.19° were indexed to (100), (110), (200), and (210) reflections, identifying its well-ordered hexagonal pore structure (Figure 5a).[8,16,28] The peak at (100) reflection of MCM-41-S catalysts shifted

toward higher 2θ values and its intensity decreased with increasing STA amount. The shift of the peak at (100) reflection toward higher 2θ values indicates the condensation of silanol groups.[16] The decrease in the intensity of these peak values with increasing STA loading indicated a decrease in the long-range order of MCM-41.[28−30] As previously mentioned, the hydrothermal method applied in the syntheses requires simultaneous addition of the active material and the silica source. It was thought that an interaction between anion species of STA and the silanol group inside the pores of MCM-41 had occurred during synthesis, which had resulted in partial destruction of MCM-41-S catalysts' mesoporous structure (Figure 5a).[29,30]

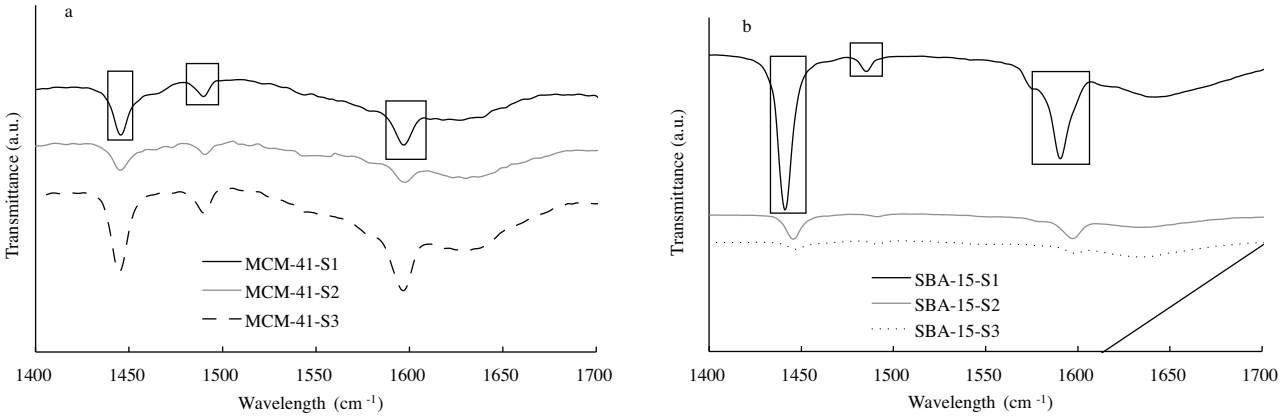

Figure 4. DRIFT analyses conducted on a) MCM-41-S and b) SBA-15-S catalysts.

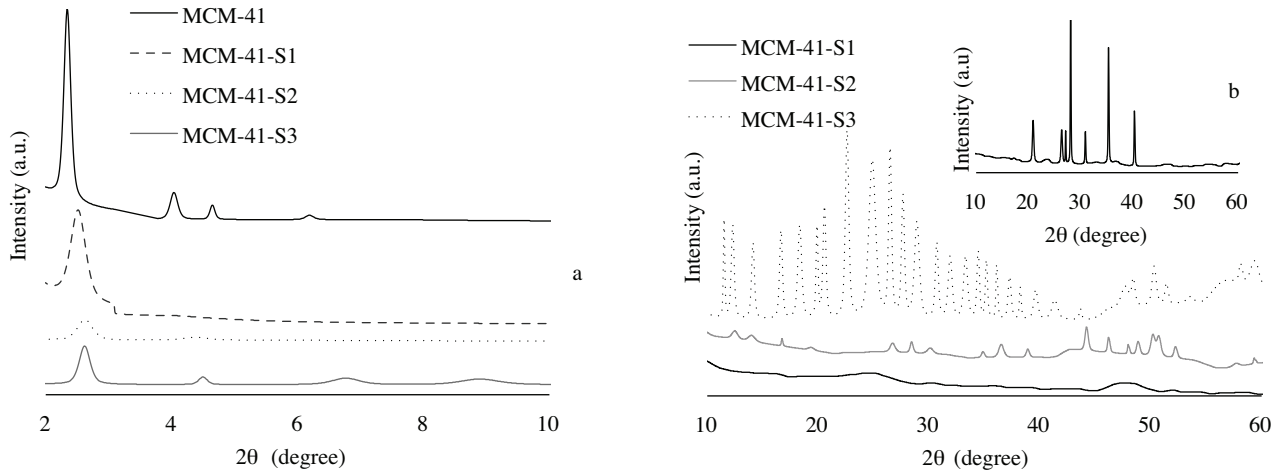

Figure 5. a) Low-angle XRD patterns of MCM-41 with MCM-41-S catalysts b) High-angle XRD patterns of STA (small figure) and MCM-41-S catalysts.

High angle XRD patterns of MCM-41-S2 and MCM-41-S3 catalysts revealed the presence of a bulk STA crystal phase (Figure 5b). It was interesting to observe diffraction patterns of the crystalline STA structure considering the applied loading amounts. As a consequence, homogeneous dispersion of STA inside the mesopores could only be achieved with MCM-41-S1 catalyst. In our opinion, the drawback that occurred in the dispersion of active material was due to the applied synthesis method, which induced condensation of silanol groups and resulted in the formation of a more compact structure (Figure 5b).[16] This compact structure, determined with low angle XRD patterns (Figure 5a), prevented migration of STA inside mesoporous channels and caused them to agglomerate on the surface of the catalyst.

The XRD patterns of low angle SBA-15 and SBA-15-S catalysts are given in Figure 6a. The XRD patterns of parent SBA-15 indicated three peak values identified at 0.93, 1.46, and 1.68°, which corresponded to (100), (110), and (200) reflections of the hexagonal mesoporous structure.[14,17,20] The (100) reflection of SBA-15-S1 catalyst shifted toward lower 2θ angles, indicating a strong interaction of STA with surfactant during the hydrothermal process.[21] Low angle XRD patterns of SBA-15-S2 and SBA-15-S3 catalysts indicated disappearance of the peak for (100) reflection, whereas the peaks corresponding to (110) and (200) reflections could clearly be observed. This result was thought to be due to increasing STA amount inside the pores of the catalysts. The fact that the (110) and (200) reflections remained despite increasing STA amount indicated that SBA-15 had kept its mesoporous structure (Figure 6a).[17] High angle XRD patterns of SBA-15-S catalysts indicated that the bulk crystal STA phase was only observed for SBA-15-S3 catalysts (Figure 6b). Comparison of high angle XRD patterns of MCM-41-S (Figure 5b) and SBA-15-S (Figure 6b) catalysts revealed the presence of greater amounts of STA inside the pores of SBA-15-S catalysts, which also explained the increase in catalytic activity with increasing W/Si% loadings.

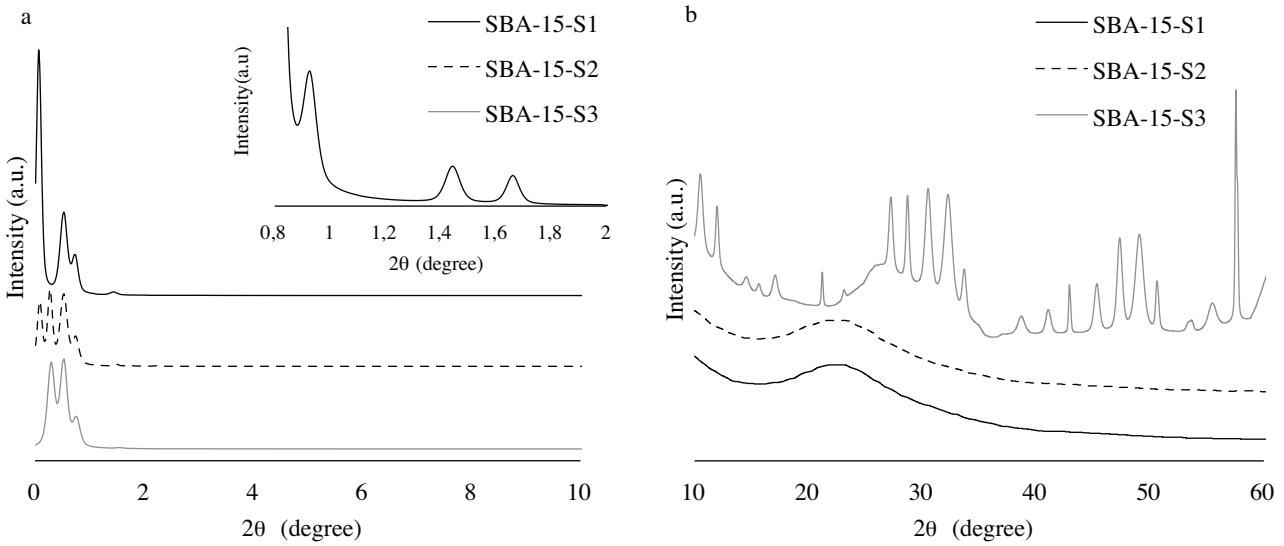

Figure 6. a) Low-angle XRD patterns of SBA-15 (small figure) and SBA-15-S catalysts b) High-angle XRD patterns of SBA-15-S catalysts.

The textural and structural properties of MCM-41-S and SBA-15-S catalysts are illustrated in Table 1 along with parent MCM-41 and SBA-15. Comparison of the surface areas of fresh MCM-41-S and SBA-15-S catalysts revealed a decrease in surface areas with increasing STA amount, as expected. A decrease in surface areas compared to fresh catalysts was also observed for spent catalysts, which was thought to be due to adsorbed reactants in the pores during the reaction. It would be best to compare the pore volumes and pore diameters of fresh and spent catalysts in order to evaluate the effect of reactants on mesoporous structure. As seen from the table, fresh SBA-15-S catalysts had higher pore volumes and pore diameters than MCM-41-S catalysts, which enabled diffusion of higher STA to its mesopores during hydrothermal synthesis. This result also explained the steady increase in activity with increasing STA amount in the presence of SBA-15-S catalysts. A drastic decrease in pore volumes and a drastic increase in pore diameters were determined for spent MCM-41-S catalysts, whereas a negligible change in these parameters was observed for spent SBA-15-S catalysts. The results obtained for spent MCM-41-S catalysts indicated that the reactants had diffused and had

adsorbed inside the mesopores of MCM-41-S catalysts and had deteriorated the pore structure in the process. The d (100) values, derived from XRD results, increased with increasing STA amount in the case of fresh MCM-41-S catalysts. Moreover, multilayer coverage of STA on the structure was observed for MCM-41-S catalysts, evidencing that most of STA remained outside mesopores during synthesis.[20] Comparison of d (100) values of spent MCM-41-S catalysts revealed a drastic increase, implying deposition of reactants on the structure after the reaction. In the case of SBA-15-S catalysts, the d (100) values of SBA-15-S1 and SBA-15-S2 indicated a monolayer coverage of STA on the structure.[20] On the other hand, accumulation of some STA on the catalyst surface was observed for SBA-15-S3 catalyst, which was previously shown in high angle XRD results (Figure 6b). The change in d (100) values between fresh and spent SBA-15-S1 and SBA-15-S2 catalysts was negligible. This result led to two conclusions. The amount of STA that migrated from the pores during the reaction could be considered negligible and the pore structure of the catalysts remained intact even after the reaction.

Table 1. Physical properties of MCM-41-S and SBA-15-S catalysts compared with MCM-41 and SBA-15.

Catalyst	BET surface area (m^2/g)		Pore volume (cm^3/g)		Pore diameter (nm)		d(100) (nm)	
	F*	S**	F	S	F	S	F	S
MCM-41	1185	-	1.2	-	2.9	-	3.9	-
MCM-41-S1	901	464	0.8	0.26	2.8	12.9	17.8	314.4
MCM-41-S2	630	604	0.5	0.33	3.0	9.9	58.7	142.9
MCM-41-S3	655	563	0.9	0.18	2.7	10.6	56.7	46.0
SBA-15	812	-	1.3	-	7.9	-	9.6	-
SBA-15-S1	860	771	1.3	1.0	7.0	7.8	15.1	11.7
SBA-15-S2	879	833	1.3	1.3	7.5	7.2	11.1	11.7
SBA-15S3	663	787	1.1	1.2	9.1	7.6	47.4	11.9

*F: fresh catalyst

**S: spent catalyst

A type IV isotherm was observed for fresh MCM-41-S catalysts, which indicated a mesoporous structure (Figure 7a).[6] The deterioration of the isotherm in the case of spent catalysts implied some deformation of pore structure during the reaction (Figure 7b). The pore structure was thought to deteriorate as a result of diffusing reactants during the reaction. The extent of deformation on the pore structure was inconclusive as the catalysts were still active in repeated use. Furthermore, a shift from mesoporous to macroporous state should have been observed in the pore size distribution of spent MCM-41-S catalysts if there had been a complete destruction of pore structure (Figure 8a and 8b). SBA-15-S catalysts also exhibited a type IV isotherm (Figure 9a) and no deterioration was observed in the isotherm of spent catalysts (Figure 9b). This result indicated that the pore structure of SBA-15-S catalysts remained intact after the reaction and was in accordance with the results obtained with XRD analyses. As expected, the SBA-15-S catalysts preserved their mesoporosity after the reaction (Figure 10a and 10b).

SEM images of MCM-41 with spent MCM-41-S catalysts and SBA-15 with spent SBA-15-S catalysts are illustrated in Figures 11 and 12, respectively. The deformation of MCM-41-S catalysts due to interaction with reactants during ethyl acetate production can clearly be observed from the images (Figures 11a–11d). On the other hand, STA addition had no significant effect on the wheat-like morphology of SBA-15 and the morphology of the catalysts remained unchanged even after the reaction (Figures 12a–12d).[18]

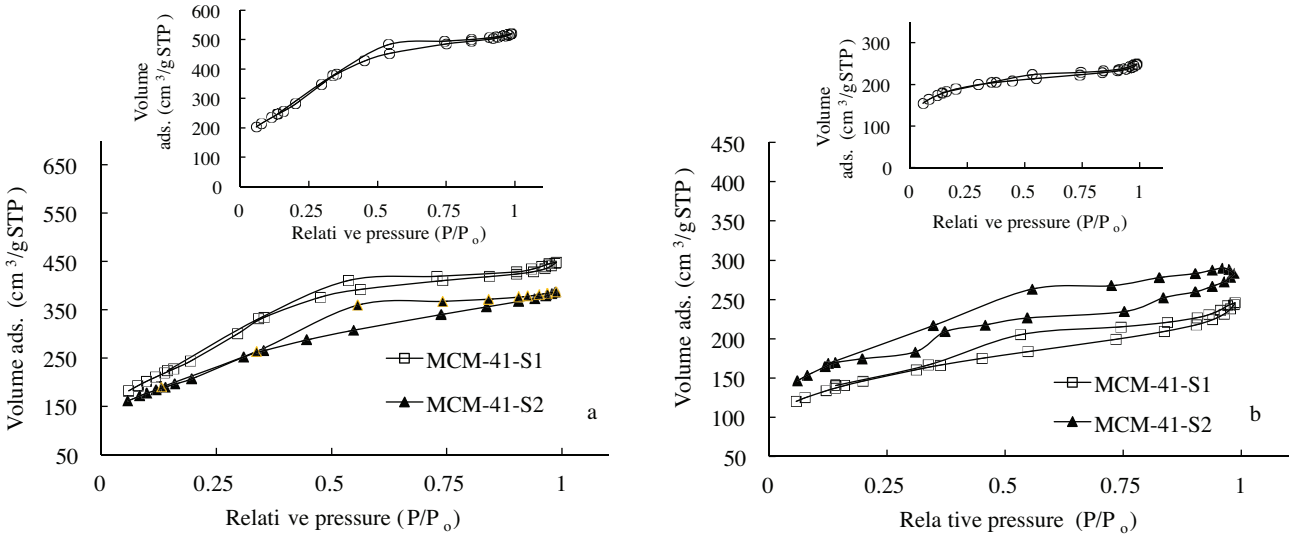

Figure 7. N_2 adsorption–desorption isotherms of a) fresh MCM-41-S1, MCM-41-S2, and MCM-41-S3 (small figure) catalysts b) spent MCM-41-S1, MCM-41-S2, and MCM-41-S3 (small figure) catalysts.

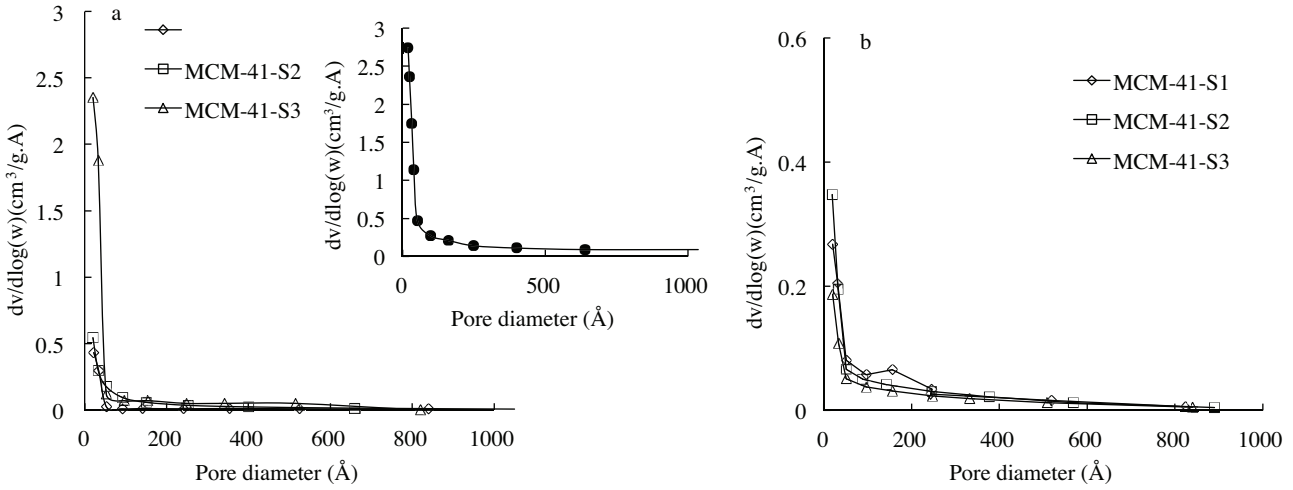

Figure 8. Pore size distributions of a) parent MCM-41 (small figure) and fresh MCM-41-S catalysts and b) spent MCM-41-S catalysts.

The results indicated that SBA-15-S catalysts preserved their structural integrity during the ethyl acetate reaction. However, preservation of STA inside the catalyst was equally important to maintain sustainable activity of the catalysts. In order to determine the extent of STA leaching from the catalyst structure, STA amounts of SBA-15-S catalysts before and after reaction were determined by EDX analyses (Table 2). The results indicated that theoretical values of STA determined prior to synthesis had been achieved. W/Si% ratios obtained after reaction clearly showed that the loss of active material in SBA-15-S1 and SBA-15-S2 catalysts was negligible. On the other hand, nearly half of the STA had migrated from the catalyst structure in SBA-15-S3 catalyst. These results were also in accordance with high angle XRD patterns evidencing the presence of crystal STA on the surface of SBA-15-S3 catalyst.

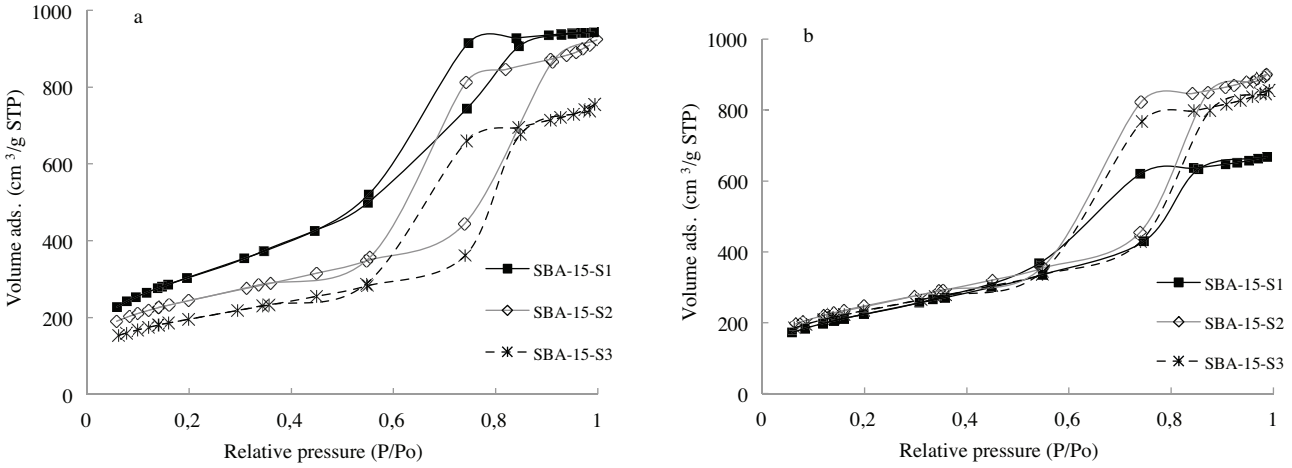

Figure 9. N_2 adsorption–desorption isotherms of a) fresh SBA-15-S catalysts and b) spent SBA-15-S catalysts.

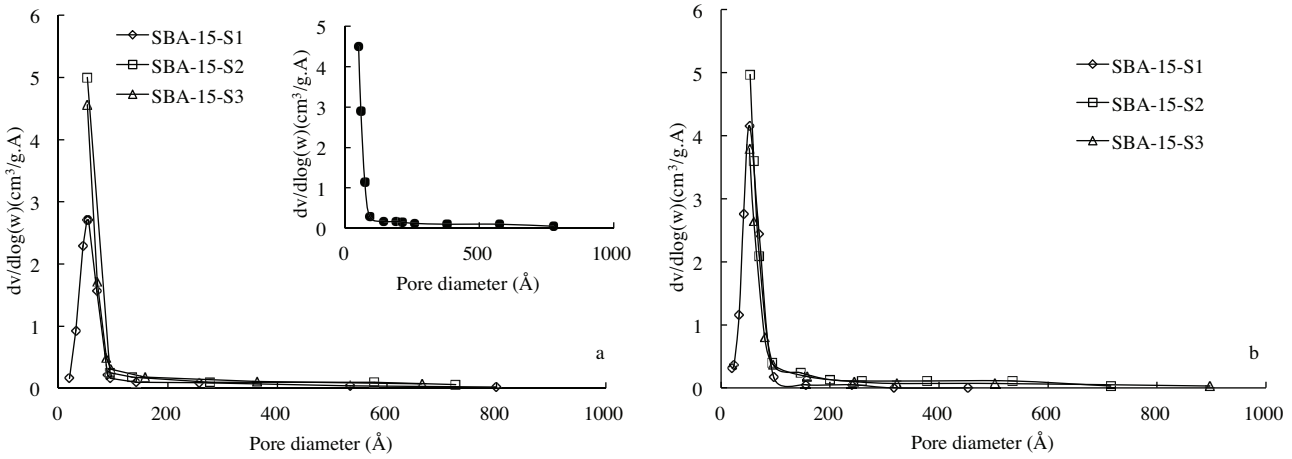

Figure 10. Pore size distributions of a) parent SBA-15 (small figure) and fresh SBA-15-S catalysts and b) spent SBA-15-S catalysts.

Table 2. W/Si % ratios of fresh and spent SBA-15-S catalysts determined with EDX analysis.

W/Si Theoretical (%)	Element	Weight (%)		W/Si Experimental (%)	
		F*	S**	F	S
1.25	W	0.3	2.8	1.0	0.9
	Si	31.0	29.6		
2.5	W	0.9	0.6	2.7	1.8
	Si	33.1	32.4		
5	W	0.5	0.8	5.0	2.3
	Si	10.0	33.1		

*F: fresh catalyst

**S: spent catalyst

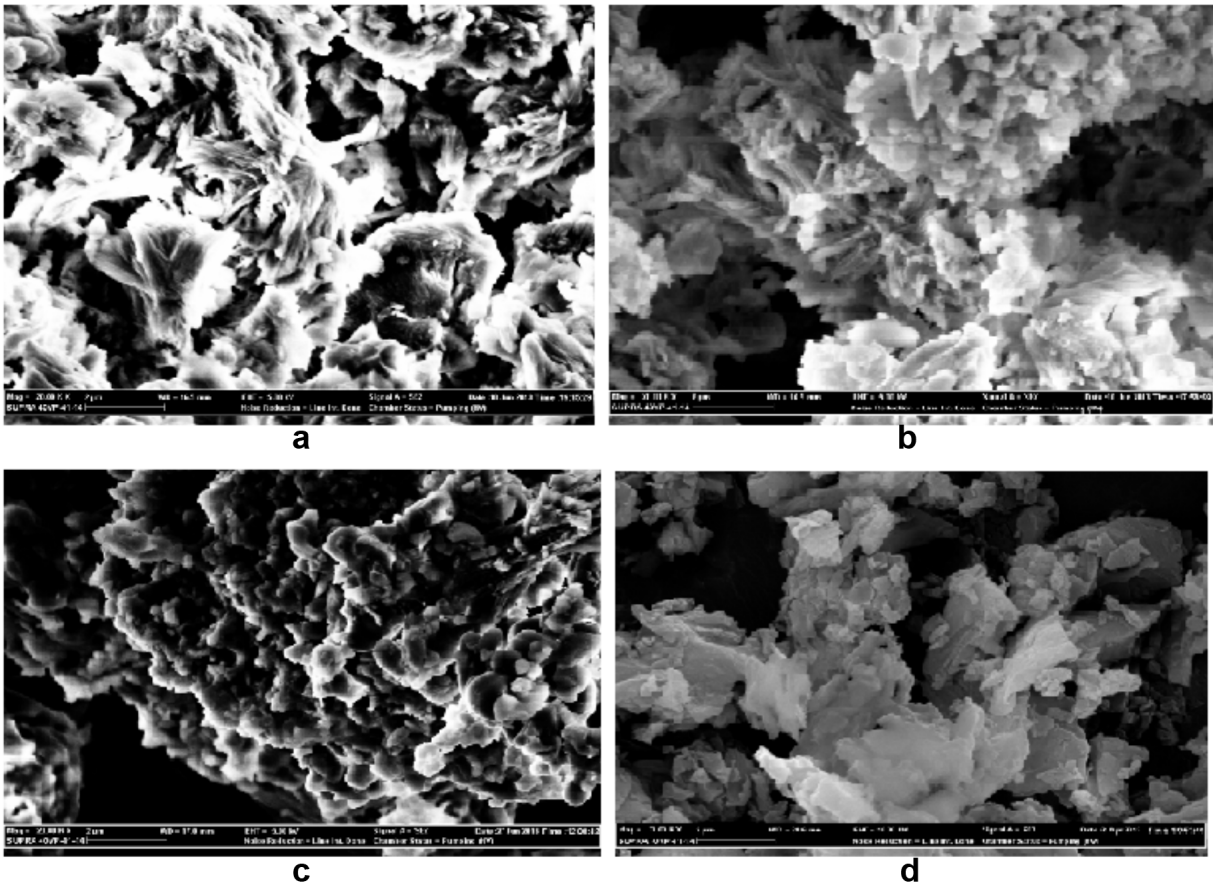

Figure 11. SEM images (20 kx) of a) spent MCM-41-S1 b) spent MCM-41-S2 c) spent MCM-41-S3 catalysts and d) fresh MCM-41.

The hydrothermal method was successfully applied in the synthesis of mesoporous silicates containing STA. The results obtained from characterization studies indicated that STA could be accumulated inside the pore structure up to a loading level of 1.25% W/Si for MCM-41-S catalysts and 2.5% W/Si for SBA-15-S catalysts. In the case of exceeding loading amounts STA was deposited on the surface of silicate. The deposition of STA on the surface of catalysts was shown by evaluation of XRD results and nitrogen physisorption experiments. Ethyl acetate production conducted in the presence of SBA-15-S catalysts showed an increase in activity with increasing W/Si% loadings. The nonmonotonic dependence of acetic acid conversion in the presence of MS catalysts was due to condensation of silanol groups in the course of synthesis. Hence, a more compact structure that prevented incorporation of STA inside the channels of the catalyst occurred with the applied synthesis method.

Comparison of MCM-41 and SBA-15 catalysts showed that SBA-15 based catalysts had been more stable during the reaction. The activities of MCM-41-S and SBA-15-S catalysts were similar. However, it was concluded that the molecular structure of SBA-15 based catalysts would be preserved in long-term use in reactions. The hydrothermal method applied in the syntheses enabled incorporation of STA up to a certain loading amount: 2.5% for MCM-41-S catalysts and 5% for SBA-15-S catalysts, which were low compared with the loading amounts applied in impregnation. On the other hand, this method was shown to prevent leaching of STA to a certain extent from the catalyst structure and the reaction results showed that considerable activities had been obtained in the reaction.

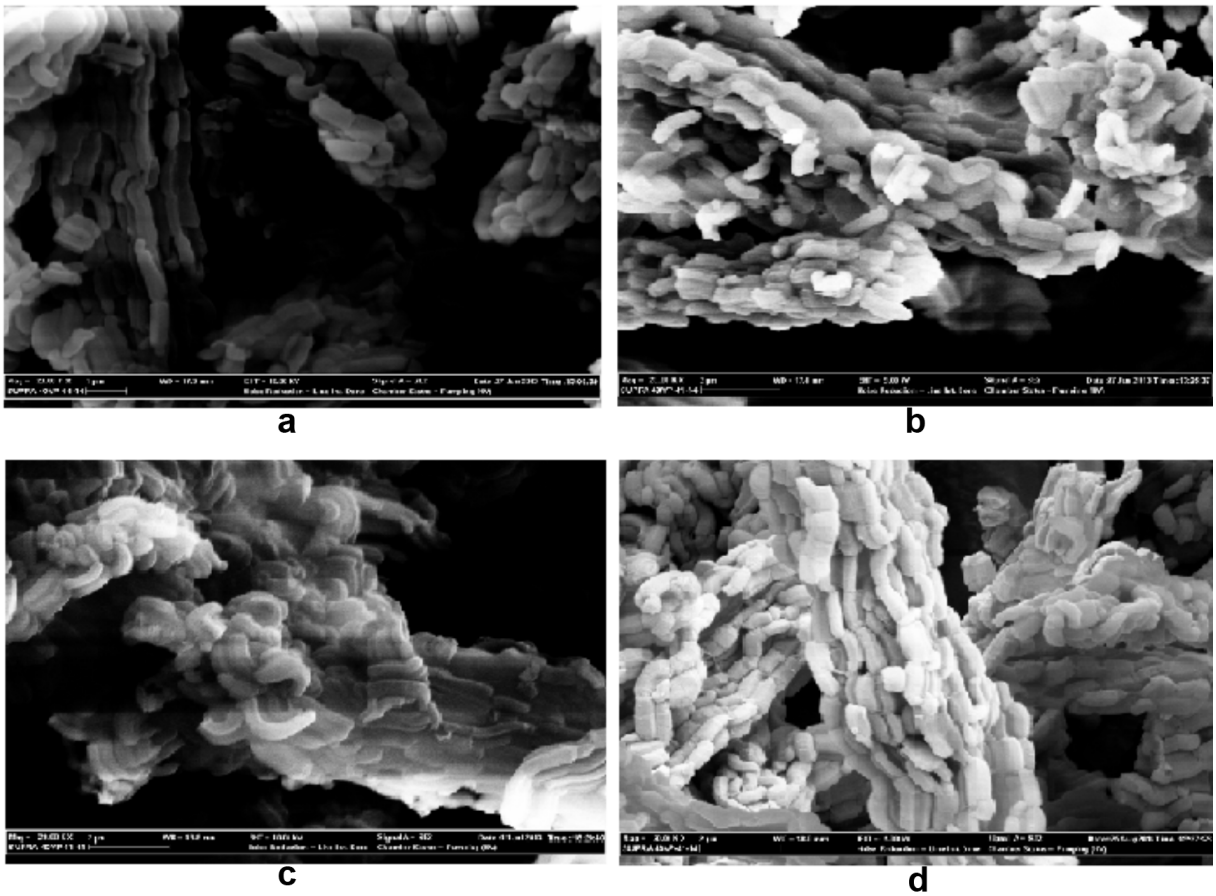

Figure 12. SEM images (20 kx) of a) spent SBA-15-S1 b) spent SBA-15-S2 c) spent SBA-15-S3 catalysts and d) fresh SBA-15.

3. Experimental studies

3.1. Synthesis of the catalysts

The hydrothermal method requiring simultaneous addition of the active material and the silicate source was applied by modification of the procedures applied previously for the synthesis of MCM-41[31] and SBA-15.[32] In the synthesis of MCM-41 based catalysts, silicotungstic acid (STA) (Sigma-Aldrich) and sodium silicate (Sigma-Aldrich) solution were employed as the active material and silicate source, respectively. Initially, a solution of a surface active material, cetyl-N, N, N-trimethylammonium bromide (CTMABr) (Merck), was prepared by addition of 13.2 g of CTMABr to 87 mL of deionized water in the synthesis of MCM-41 based catalysts. This solution was stirred at 30 °C until a transparent solution was obtained. A 27% (w/w) solution of sodium silicate and STA were added dropwise to this transparent solution. The pH value of STA containing solution was adjusted to 11 and the solution was stirred for another hour and placed in an autoclave to be aged for 96 h at 120 °C. The obtained gel was separated from the sample by filtration and the sample was washed with deionized water to decrease the pH to 7. The sample was dried at 30 °C for 18 h and then calcined at 350 °C for 6 h in a tubular furnace for removal of the surfactant. Calcination temperature was determined based on the physical properties of STA. The STA amounts utilized in synthesis were determined as 1.25%, 2.5%, and 5% based on weight ratio of tungsten (W) of STA to silicium (Si) of sodium silicate solution (W/Si). MCM-41

based catalysts synthesized by this procedure were named MCM-41-S1, MCM-41-S2, and MCM-41-S3 based on increasing W/Si % ratios.

Synthesis of SBA-15 based catalysts was conducted in acidic conditions: $1 < pH < 2$. Initially, 4 g of triblock copolymer surfactant, Pluronic P123 (Sigma-Aldrich), was dissolved in 144 mL of 1.7 M HCl at 40 °C. The solution was stirred for 4 h before simultaneous addition of tetraethylorthosilicate (TEOS, Merck) and STA. The molar ratio of TEOS/Pluronic P123 was determined as 2 in the course of syntheses. The resulting solution was further stirred for 2 h and aged at 100 °C for 48 h. The formed crystalline sample was washed with deionized water, dried at 80 °C for 12 h, and finally calcined at 350 °C for 5 h in a tubular furnace for removal of the surfactant. The amounts of STA added to the catalysts were identical with those used in the syntheses of MS catalysts. The synthesized catalysts were named SBA-15-S1, SBA-15-S2, and SBA-15-S3 based on increasing W/Si % ratios.

3.2. Reaction experiments

The activity of the catalysts was determined by ethyl acetate production selected as the model reaction. Reaction experiments were conducted in a batch reactor equipped with a reflux condenser. Catalyst amount and temperature were determined as 0.4 g and 343 K, respectively. Ethanol/acetic acid molar ratio was determined as 1/1 and the reactions were conducted under identical conditions. Analyses of reactants and product were performed in a gas chromatograph equipped with a FID detector and a TRB Wax 30 m $\times$ 0.32 $\times$ 0.5 μm capillary column.

Catalysts recovered after the first run were washed three times with deionized water and dried at 90 °C for 3 h. The activity of these recovered catalysts was also tested in ethyl acetate production conducted under identical conditions. The catalysts recovered after this second run were utilized in characterization studies to examine the changes that might have occurred in their molecular structure.

3.3. Characterization studies

In order to determine the acidic property of the catalysts, the samples were initially treated with pyridine and then analyzed by diffuse reflectance FT-IR (DRIFTS). Experiments were conducted on a PerkinElmer instrument in the range of 380–4000 cm^{-1}. XRD patterns of MCM-41-S and SBA-15-S catalysts were obtained on a Panalytical Empryran HT-XRD instrument using CuK_α radiation with 0.066 step size and over the range $0° < 2\theta < 10°$. Adsorption–desorption isotherms and pore size distributions of fresh and spent MCM-41-S and SBA-15-S catalysts were obtained by nitrogen physisorption analyses conducted in an ASAP2020 instrument. BET and BJH methods were evaluated in accordance with XRD results. SEM images of fresh and spent catalysts were obtained with a Zeiss SUPRA V 40 device. EDX analyses were applied to fresh and spent catalysts to determine the extent of leaching of the active material during syntheses and/or reaction experiments. MCM-41 and SBA-15 were also synthesized and analyzed to determine the validity of the applied procedures and the changes that occurred in their structure by STA addition.

Acknowledgments

The financial contributions from Gazi Research Funds (06/2012-47 and 06/2012-18) and the Scientific and Technological Research Council of Turkey (TÜBİTAK 114M005) are gratefully acknowledged.

References

1. Kusuma, R. I.; Hadinoto, J. P.; Ayucitra, A.; Soetaredjo, F. E.; Ismadji, S. *App. Clay Sci.* **2013**, *74*, 121–126.
2. Li, B.; Li, H.; Weng, W. Z.; Zhang, Q.; Huang, C. J.; Wan, H. L. *Fuel* **2013**, *103*, 1032–1038.
3. Tokay, K. C.; Dogu, T.; Dogu, G. *Chem. Eng. J.* **2012**, *184*, 278–285.
4. Obalı, Z.; Dogu, T. *Chem. Eng. J.* **2008**, *138*, 548–555.
5. Degirmenci, L.; Oktar, N.; Dogu, G. *AlChe J.* **2011**, *57*, 3171–3181.
6. Yang, K.; Peng, J.; Srinivaskannan, C.; Zhang, L.; Xia, H.; Duan, X. *Bioresource Tech.* **2010**, *101*, 6163–6169.
7. Thieleman, J. P.; Girgsdies, F.; Schlögl, R.; Hess, C. *Beilstein Journal of Nanotech.* **2011**, *2*, 110–118.
8. Wang, J. A.; Chen, L. F.; Norena, L. E.; Navarrate, J.; Llanos, M. E.; Contreras, J. L.; Novaro, O. *Microporous and Mesoporous Materials* **2008**, *112*, 61–76.
9. Ghiaci, M.; Aghabarari, B. *Chinese Journal of Catalysts* **2010**, *31*, 759–764.
10. Llanos, A.; Melo, L.; Avendano, F.; Montes, A.; Brito, J. L. *Catalysis Today* **2008**, *133-135*, 20–27.
11. Varışlı, D.; Tokay, K. C.; Çiftçi, A.; Doğu, T.; Doğu, G. *Turk J. Chem.* **2009**, *33*, 355–366.
12. Varisli, D.; Dogu, T.; Dogu, G. *Chem. Eng. Sci.* **2010**, *65*, 153–159.
13. Degirmenci, L.; Oktar, N.; Dogu, G. *Ind. Eng. Chem. Res.* **2009**, *48*, 2566–2576.
14. Brahmkhatri, V.; Patel, A. *Fuel* **2012**, *102*, 72–77.
15. Li, B.; Ma, W.; Liu, J.; Zuo, S.; Li, X. *Journal of Colloid and Interface Science* **2011**, *362*, 42–49.
16. Mendez, F.; Llanos, A.; Echeverria, M.; Jauregui, R.; Villasana, Y.; Diaz, Y.; Liendo-Polanco, G.; Ramos-Garcia, M. A.; Zoltan, T.; Brito, J. L. *Fuel* **2013**, *10*, 249–258.
17. Liu, Q. Y.; Wu, W. L.; Wang, J.; Ren, X. Q.; Wang, Y. R. *Microporous and Mesoporous Materials* **2004**, *76*, 51–60.
18. Sawant, D. P.; Vinu, A.; Jacob, N. E.; Lefebvre, F.; Halligudi, S. B. *Journal of Catalysis* **2005**, *235*, 341–352.
19. Sawant, D. P.; Vinu, A.; Mirajkar, S. P.; Lefebvre, F.; Ariga, K.; Anandan, S.; Mori, T.; Nishimura, C.; Halligudi, S. B. *Journal of Molecular Catalysis A: Chemical* **2007**, *271*, 46–56.
20. Kumar, G. S.; Vishnuvarthan, M.; Palanichamy, M.; Murugesan, V. *Journal of Molecular Catalysis A: Chemical* **2006**, *260*, 49–55.
21. Yang, L.; Qi, Y.; Yuan, X.; Shen, J.; Kim, J. *Journal of Molecular Catalysis A: Chemical* **2005**, *229*, 199–205.
22. Merchant, S. Q.; Almohammad, K. A.; Bassam, A. A. M.; Ali, S. H. *Fuel* **2013**, *111*, 140–147.
23. El- Wahab, M. M. M. A.; Said, A. A. *Journal of Molecular Catalysis A: Chemical* **2005**, *240*, 109–118.
24. Gurav, H.; Bokade, V. V. *Journal of Natural Gas Chemistry* **2010**, *19*, 161–164.
25. Dai, Q.; Wang, X.; Chen, G.; Zheng, Y.; Lu, G. *Microporous and Mesoporous Materials* **2007**, *100*, 268–275.
26. Varisli, D.; Dogu, T.; Dogu, G. *Ind. Eng. Chem. Res.* **2008**, *47*, 4071–4076.
27. Varisli, D.; Dogu, T.; Gulsen, D. *Ind. Eng. Chem. Res.* **2009**, *48*, 9394–9401.
28. Karthikeyan, G.; Pandurangan, A. *Journal of Molecular Catalysis A: Chemical* **2009**, *311*, 36–45.
29. Chen, Y.; Dong, B. B.; Wang, G. H.; Zheng, X. C. *Materials Letters* **2014**, *114*, 72–75.
30. Ahmed, A. I.; Samra, S. E.; El-Hakam, S. A.; Khder, A. S.; El-Shenawy, H. Z. *Applied Surface Science* **2013**, *282*, 217–225.
31. Sener, C.; Dogu, T.; Dogu, G. *Microporous and Mesoporous Materials* **2006**, *94*, 89–98.
32. Fulvio, P. F.; Pikus, S.; Jaroinec, M. *Journal of Colloid and Interface Science* **2005**, *287*, 717–720.